The effect of voxel size on high-resolution peripheral computed tomography measurements of trabecular and cortical bone microstructure

Willy Tjong,[a] Galateia J. Kazakia,[b] Andrew J. Burghardt,[c] and Sharmila Majumdar[d]
*Musculoskeletal Quantitative Imaging Research Group, Department of Radiology and Biomedical Imaging,
University of California, San Francisco, San Francisco, California 94107*

Purpose: Accurate quantification of bone microstructure plays a significant role in understanding bone mechanics and response to disease or treatment. High-resolution peripheral quantitative computed tomography (HR-pQCT) allows for the quantification of trabecular and cortical structure *in vivo*, with the capability of generating images at multiple voxel sizes (41, 82, and 123 μm). The aim of this study was to characterize the effect of voxel size on structural measures of trabecular and cortical bone and to determine accuracy in reference to micro-CT (μCT), the gold standard for bone microstructure quantification.
Methods: Seventeen radii from human cadaver specimens were imaged at each HR-pQCT voxel size and subsequently imaged using μCT. Bone density and microstructural assessment was performed in both the trabecular and cortical compartments, including cortical porosity quantification. Two distinct analysis techniques were applied to the 41 μm HR-pQCT data: the standard clinical indirect analysis and a direct analysis requiring no density or structural model assumptions. Analysis parameters were adjusted to enable segmentation and structure extraction at each voxel size.
Results: For trabecular microstructural measures, the 41 μm HR-pQCT data displayed the strongest correlations and smallest errors compared to μCT data. The direct analysis technique applied to the 41 μm data yielded an additional improvement in accuracy, especially for measures of trabecular thickness. The 123 μm data performed poorly, with all microstructural measures either having moderate or nonsignificant correlations with μCT data. Trabecular densitometric measures showed strong correlations to μCT data across all voxel sizes. Cortical thickness was strongly correlated with μCT values across all HR-pQCT voxel sizes. The accuracy of cortical porosity parameters was highly dependent on voxel size; again, the 41 μm data was most strongly correlated. Measures of cortical density and pore diameter at all HR-pQCT voxel sizes had either weak or nonsignificant correlations.
Conclusions: This study demonstrates the effect of voxel size on the accuracy of HR-pQCT measurements of trabecular and cortical microstructure and presents parameters for HR-pQCT analysis at nonstandard resolutions. For all parameters measured, correlations were strongest at 41 μm. Weak correlations for porosity measures indicate that a better understanding of pore structure and resolution dependence is needed. © *2012 American Association of Physicists in Medicine*. [http://dx.doi.org/10.1118/1.3689813]

I. INTRODUCTION

The emergence of high-resolution peripheral computed tomography (HR-pQCT) as a viable imaging modality has allowed for the *in vivo* analysis of bone structure parameters at a level approaching microstructural dimensions. The ability of HR-pQCT to accurately assess bone structure has important clinical implications. Though bone mineral density (BMD) is currently accepted as the most significant predictor of fracture risk, recent efforts have been made to include the contribution of other measures of bone quality, including macro- and microarchitectural parameters.[1,2] Proper assessment of these parameters, therefore, is paramount to further delineating the factors that affect risk of fracture.

Microcomputed tomography (μCT) has been established as the gold standard for bone microstructural measurements.

Driving the difference between HR-pQCT and μCT for measures of bone microstructure is a difference in imaging resolution. Whereas the newest generation of μCT systems can generate images with a voxel size as small as 0.5 μm with a spatial resolution of less than 2 μm (10% MTF), the standard imaging protocol for HR-pQCT results in images with a voxel size of 82 μm, with a spatial resolution of approximately 130–140 μm (10% MTF). To account for such a large disparity in image resolution, analysis techniques specific to each imaging system have been developed to measure cortical and trabecular parameters.[3–11] The high resolution of μCT images relative to typical trabecular dimensions allows for direct voxel-based measurement of bone volume (BV/TV) as well as trabecular number (Tb.N), thickness (Tb.Th), and separation (Tb.Sp). To compensate

for the lower resolution of HR-pQCT images, an indirect analysis method was developed[4]; in the standard clinical analysis, only Tb.N is directly measured while other parameters are derived using various assumptions.

While previous studies have examined the accuracy of HR-pQCT images at 82 μm voxel size,[6,12,13] little attention has been paid to the accuracy of the HR-pQCT system at other nominal resolutions. In addition to the standard clinical protocol at a voxel size of 82 μm, HR-pQCT can also generate images with voxel sizes of 41 and 123 μm. Although several *in vitro* studies have made use of imaging at 41 μm, the extent to which HR-pQCT measures derived at 41 μm correlate to those derived from μCT has yet to be fully investigated. Considering the smaller voxel size of images at 41 μm, it is possible that these images generate more accurate measures than standard 82 μm images. If analysis of images at 123 μm voxel size reasonably approximates μCT data, then the computational cost and processing time for image analysis would be greatly reduced in addition to shorter scan times and lower radiation dose for patient scans.

The analysis of HR-pQCT images at various voxel sizes provides an estimate of the resolution dependence of the calculated bone parameters. For trabecular parameters, this dependence has been explored by comparing HR-pQCT analysis to gold standard μCT data.[6,13] No similar study has been carried out on newly developed extended cortical structure and porosity measures.[8] Cortical porosity measures attempt to characterize normal physiological pore space (e.g., Haversian canals) as well as the pathological macroporosity recently described in osteopenic populations.[14] Though a previous study has compared porosity measures calculated from μCT and 82 μm HR-pQCT images,[11] the cortical analysis technique used in that study has since been refined to provide better estimates of porosity. The optimal resolution for measuring porosity might be different than that for measuring trabecular architecture. The establishment of a μCT-based standard of reference and the evaluation of resolution effects, therefore, are both necessary to determine the accuracy of HR-pQCT cortical porosity measures. The accurate measurement of cortical porosity has significant clinical relevance, considering that changes in the cortical microstructure can significantly affect bone strength.[7,11]

The purpose of this study, therefore, is to investigate the effect of voxel size on cortical and trabecular parameters calculated from HR-pQCT with reference to μCT. To achieve this, specimens were imaged using HR-pQCT at three different voxel sizes (41, 82, and 123 μm) and using μCT at 18 μm voxel size to provide a reference. Two distinct analysis techniques were applied to the HR-pQCT data: the standard clinical indirect analysis and a direct analysis requiring no density or structural model assumptions. Analysis parameters were adjusted to enable segmentation and structure extraction at each voxel size. This work is novel in two ways. First, this study provides the first systematic examination of the accuracy of HR-pQCT analysis at nonstandard resolutions with comparison to the gold standard technique, μCT. Second, this study applies the extended cortical analysis to μCT data, which has not previously been reported.

II. METHODS

II.A. HR-pQCT spatial resolution

Spatial resolution at each voxel size was measured in the tomographic plane for image data acquired from a custom-built wire phantom (QRM GmbH, Möhrendorf, Germany) designed to approximate the point spread function (PSF). The phantom consisted of an 8 cm diameter cylinder of soft-tissue equivalent polymer resin with a 25 μm diameter tungsten wire embedded at the center and oriented parallel to the long axis. The wire was positioned approximately near the center of rotation during acquisition. Scanning parameters for the acquisition at each voxel size were identical to those used to image the specimens (described in Sec. II C). At each resolution, the spatial resolution was estimated from the PSF images of the wire phantom. A 32×32 neighborhood was identified around the approximate wire location in the central slice. A super-sampled PSF was generated by calculating the precise subvoxel position of the wire in each slice according to the method described by Kwan *et al.*[15] A normalized modulation transfer function (MTF) was calculated from the Fourier transform of the PSF. The spatial resolution was defined as the spatial frequency corresponding to 10% of the MTF height and was reported in micrometers.

II.B. Specimens

Radii were obtained from 17 human cadavers (9 male, 8 female; 60–93 years). All specimens were received fresh frozen from National Disease Research Interchange (NDRI, Philadelphia, PA) and were kept frozen until 12 h before scanning. All specimens had partial soft tissue covering sections of the radius.

II.C. HR-pQCT imaging

Intact specimens were initially imaged using a clinical HR-pQCT scanner (XtremeCT, Scanco Medical AG, Brütti-sellen, Switzerland) with the X-ray source potential set to 60 kVp and a current of 900 μA. The remaining parameters for each scan varied depending on the desired voxel size. For images with an isotropic voxel size of 82 μm, 750 projections were acquired at a 100 ms integration time/projection. The 126 mm field of view (FOV) was then reconstructed across a 1536×1536 matrix, yielding the desired voxel size. For images with an isotropic voxel size of 41 μm, 1000 projections were acquired at a 200 ms integration time/projection and subsequently reconstructed across a 3072×3072 matrix. For images with a voxel size of 123 μm, 500 projections were acquired at a 100 ms integration time/projection and subsequently reconstructed across a 1024×1024 matrix. The size of the detector was 3072×256; therefore, the projection images at 41 μm had no binning while the projection images at 82 and at 123 μm were subjected to 2×2 and 3×3 binning, respectively.

Specimens were scanned starting at a location 9.5 mm proximal to the distal endplate, covering a distance of 9.02 mm in the proximal direction. Images consisted of 73 slices (yielding a voxel size of 9.02 mm/73 slices = 123 μm),

110 slices (82 µm), and 220 slices (41 µm). The linear attenuation values generated from the reconstructions were converted to hydroxyapatite (HA) mineral densities using calibration data derived from a phantom provided by the manufacturer.

II.D. µCT imaging

After HR-pQCT imaging, specimens were dissected (soft tissue removed) and radii were cut using a diamond blade precision saw (IsoMet 1000, Buehler, Lake Bluff, IL) to a length overlapping the HR-pQCT imaging region. Marrow was removed using successive cycles of water jet treatment and Terg-a-zyme detergent (Alconox, New York, NY) followed by sonication. Specimens were then submerged in saline and vacuum degassed. Images were acquired using a desktop *in vitro* µCT system (µCT-40, Scanco Medical AG, Brüttisellen, Switzerland) with the x-ray source potential set to 70 kVp and a current of 114 mA. 1023 projections were acquired at a 400 ms integration time/projection, and the resulting projections were reconstructed across a 2048×2048 matrix, yielding an isotropic voxel size of 18 µm. Calibration of reconstructed linear attenuation values was performed using an HA phantom supplied by the manufacturer.

II.E. Image analysis

II.E.1. Periosteal contouring

For the HR-pQCT images, contours identifying the periosteal perimeter of the bone were drawn semiautomatically using an edge-finding algorithm previously described in the literature.[4] All contours were examined manually and modified as necessary to ensure proper segmentation of bone. Periosteal contours for the µCT images were created semiautomatically by first identifying the periosteal perimeter using the edge-finding algorithm referenced above on every 25th slice and then interpolating throughout the whole sample.

II.E.2. Registration

In order to ensure that the same volume of interest (VOI) was analyzed across all image sets, the HR-pQCT and µCT image sets were spatially coregistered. For each specimen, the µCT image set was chosen as the fixed frame of reference, and each corresponding HR-pQCT image set was transformed accordingly by applying a 3D rigid transformation. To determine the transformation, all grayscale images and periosteal contours were resampled using Image Processing Language (IPL v5.08 b, Scanco Medical AG) to a voxel size of 82 µm to standardize image dimensions. Grayscale images were then aligned using Rview (http://rview.colin-studholme.net), a program that calculates a transformation matrix based on normalized mutual information.[16] This transformation was applied to the HR-pQCT periosteal contours; the resulting transformed contours were subsequently overlaid with the corresponding µCT contours in IPL to extract the common region among all images. This contour consisting of the union between all four image sets then

inverse transformed and resampled as necessary to define the registered VOI for each HR-pQCT resolution.

Because of imprecision in the tissue cutting process, the full HR-pQCT volume was not available for analysis in the µCT data set. Those samples that had less than a 50% overlap of slices were discarded, resulting in a total of 14 samples that were suitable for analysis. All subsequent analysis was performed on the registered VOI of each specimen.

II.F. Image analysis—trabecular compartment

II.F.1. HR-pQCT standard analysis (indirect)

HR-pQCT images were evaluated using the standard clinical evaluation protocol.[4] In the standard protocol developed for 82 µm images, the cortical compartment is initially identified by a two-step process that applies a Gaussian filter followed by a threshold-based segmentation. The trabecular compartment is then segmented by subtraction of the cortical region from the periosteal region. The parameters of this process required adjustment to reasonably separate cortical and trabecular compartments in the 41 and 123 µm data sets. Images at 41 µm required a greater level of smoothing to separate the cortical compartment, while 123 µm images needed less smoothing. All segmentations were checked visually to ensure that appropriate separation was achieved while preserving cortical thickness. A summary of the adjusted parameter values for the compartment segmentation at each HR-pQCT voxel size is given in Table I. Other analysis parameters dependent on voxel size were scaled as necessary for each resolution data set.

Structural extraction of the mineralized portion of bone was achieved by applying a Laplace–Hamming (L–H) filter followed by a fixed threshold binarization. Due to a difference in the noise performance of the 41 and 123 µm scan protocols, the filter and threshold parameters required adjustment. For the 41 µm images, the L–H filter was modified to increase the degree of smoothing in order to filter out noise in the trabecular compartment. For the 123 µm images, greater edge enhancement and decreased smoothing were necessary in order to maintain trabecular connectivity. Parameter values were chosen based on: (1) visual inspection of the segmentations, which were evaluated based on their ability to maintain trabecular connectivity while excluding noise; and (2) the strength of the correlations between HR-

TABLE I. Adjusted segmentation parameters for HR-pQCT images. Analysis parameters dependent on voxel size were scaled as necessary for each HR-pQCT data set.

Compartment segmentation (Gaussian filter)			Structure extraction (Laplace–Hamming filter)		
Voxel size (µm)	Sigma	Support	Epsilon	Cut-off frequency	Fixed threshold (%)
41	4	6	0.5	0.2	23
82	2	3	0.5	0.4	40
123	2	1	0.6	0.5	40

pQCT and μCT-derived structure measures. A single set of parameters was chosen for each HR-pQCT voxel size (Table I).

From the segmented image, BV/TV was calculated based on the volumetric BMD of the trabecular region (Tb.BMD), assuming a tissue mineral density of 1200 mg HA/cm^3. Tb.N was calculated directly by a model-independent sphere fitting technique.[3,10] Based on the calculated BV/TV and Tb.N values, Tb.Sp and Tb.Th were derived using standard histomorphometric relations assuming a plate model.[5,17]

II.F.2. Direct analysis

The 41 μm HR-pQCT images and the 18 μm μCT images were additionally processed by direct 3D methods for measurement of trabecular structural parameters.[6,10] Segmentation of the 41 μm HR-pQCT images was achieved as described previously for the standard clinical analysis. The μCT images were segmented by application of a Gaussian filter followed by thresholding using a value determined by an automated adaptive-iterative algorithm.[6] From this segmentation, trabecular BV/TV was calculated by direct voxel counting of the bone and background regions, and trabecular structure parameters were calculated directly using a sphere-filling model-independent technique.[18]

II.G. Image analysis—cortical compartment

II.G.1. Extended cortical bone analysis

Cortical parameters were assessed using an extended cortical bone analysis that provides a direct calculation of cortical thickness as well as measures of porosity.[8] The first step in this process is the creation of a cortical mask. For the HR-pQCT data, both the periosteal contour and the segmented image of the bone generated previously were used to create an endosteal contour through a series of dilations and erosions and the application of a connectivity filter.[8] The cortical compartment was identified by subtracting the endosteal contour from the periosteal contour. For the μCT data, computational constraints prevented the automatic generation of endosteal contours. Specifically, the memory required to perform the series of dilation operations was beyond the capability of the workstation used, so contours were created manually.

Application of the cortical mask generated above to a binary image of the bone provides an initial estimate of cortical porosity. For HR-pQCT images, the cortical mask was applied to the binary image using a L–H filter and a fixed threshold as described above in Sec. II F 1 (Table I). For μCT images, the binary image was created by applying an adaptive-iterative threshold to the original grayscale image.

The porosity segmentation is further refined by application of a 2D connectivity filter to exclude voids belonging to endosteal marrow space or extraosseal compartments along with a hysteresis region-growing process to include intra-cortical pore voxels that were not identified by the initial porosity estimate, as described in detail elsewhere.[8] Parameters for the connectivity filter dependent on voxel size were scaled as necessary for each resolution data set.

Values for the following structural parameters were then calculated: cortical bone mineral density (Ct.BMD) and tissue mineral density (Ct.TMD), cortical thickness (Ct.Th), cortical porosity (Ct.Po), and mean and standard deviation of cortical pore diameter (Ct.Po.Dm and Ct.Po.Dm.SD, respectively). Ct.BMD was calculated as the mean value of all voxels within the cortical compartment, while Ct.TMD excluded void voxels. Both density measures excluded two layers of pixels at the VOI and bone surface, respectively, to minimize bias from partial volume voxels. Both Ct.Th and Ct.Po.Dm were determined using a 3D sphere filling technique.[18] Ct.Po was defined as the fraction of the segmented pore volume over the sum of the pore and cortical bone volume.

II.H. Statistical analysis

Means and standard deviations for each structural parameter were calculated. To facilitate comparison between the HR-pQCT and μCT images, the difference of each HR-pQCT value with respect to the μCT value was also calculated. Regression analysis was performed between each pair of μCT and HR-pQCT values (μCT vs 41 μm HR-pQCT, μCT vs 82 μm HR-pQCT, and μCT vs 123 μm HR-pQCT), and the corresponding linear equations, r^2 values, and root mean square error (RMSE) were tabulated. Bland–Altman plots were generated to qualitatively assess the agreement between μCT and HR-pQCT values. The root mean square error coefficient of variation (RMSCV) was also calculated to characterize error for each parameter. To identify parameters that showed significant resolution dependence ($p < 0.05$), a repeated measures one-way analysis of variance (RMANOVA) was performed for each parameter across all voxel sizes. Those that showed resolution dependence were analyzed further using a post-hoc *t*-test. All statistical analysis was performed using JMP (Version 7.0, SAS Institute, Inc., Cary, NC).

III. RESULTS

Data for the MTF generated at each HR-pQCT voxel size are shown in Fig. 1. For a voxel size of 41 μm, the spatial resolution was calculated to be 88 μm (10% MTF); for
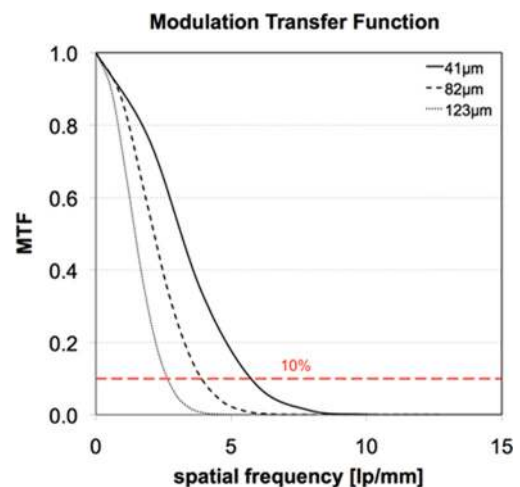

FIG. 1. MTF data for the HR-pQCT images at each voxel size.

18 μm   41 μm   82 μm   123 μm

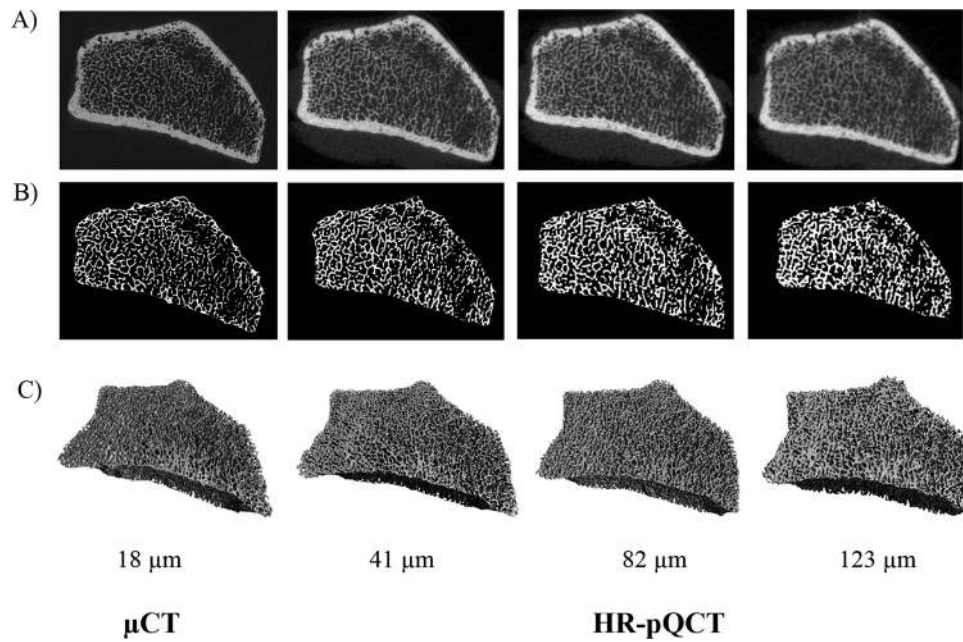**μCT**   **HR-pQCT**

FIG. 2. Representative images of the trabecular segmentation for both μCT and HR-pQCT images. (A) Grayscale images acquired by the respective scanners. (B) Trabecular segmentation of a single slice. (C) 3D representation of the trabecular volume.
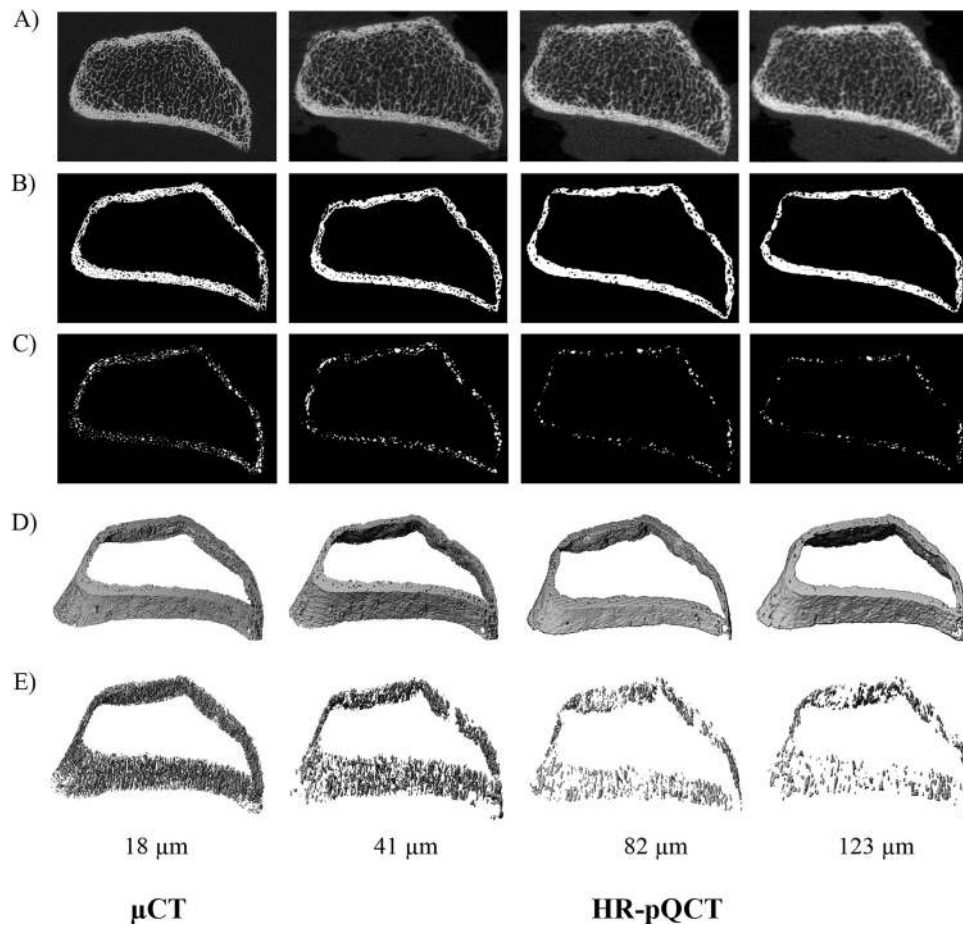

18 μm   41 μm   82 μm   123 μm

μCT   **HR-pQCT**

FIG. 3. Representative images of the cortical segmentation. (A) Grayscale images acquired by the respective scanners. (B) Cortical segmentation of a single slice. (C) Cortical porosity segmentation of a single slice. (D) 3D representations of the cortical volume. (E) 3D representations of the cortical porosity volume.

TABLE II. Regression data for trabecular parameters.

Voxel size (μm)	Slope	Intercept	r^2	RMSE
BV/TV				
41—direct	0.76	0.02	0.99	0.0051
41—indirect	0.98	0.05	0.97	0.0082
82	0.94	0.06	0.97	0.0082
123	0.88	0.07	0.96	0.0091
Tb.BMD				
41—direct	0.63	79	0.84	14.6
41—indirect	0.62	86	0.84	14.4
82	0.59	92	0.85	14.1
123	0.56	100	0.84	14.3
Tb.N				
41—direct	0.95	0.06	0.94	0.048
41—indirect	0.84	0.18	0.93	0.050
82	0.62	0.35	0.88	0.066
123	0.47	0.55	0.77	0.093
Tb.Th				
41—direct	1.01	−0.03	0.82	0.0048
41—indirect	0.39	0.13	0.48	0.0082
82	0.46	0.13	0.42	0.0086
123	0.47	0.13	0.37	0.0090
Tb.Sp				
41—direct	0.96	0.06	0.95	0.037
41—indirect	0.9	0.11	0.94	0.040
82	0.9	0.19	0.91	0.046
123	0.73	0.29	0.78	0.074

82 μm, the spatial resolution was 128 μm (10% MTF), and for 123 μm, the spatial resolution was 190 μm (10% MTF).

Representative images of the trabecular and cortical segmentation are shown in Figs. 2 and 3, respectively. Differences between the HR-pQCT images at the various voxel sizes were evident for both segmentations. For the trabecular region, a decrease in voxel size resulted in a noticeable thinning of trabeculas and increased separation. For the cortical region, decreased voxel size tended to increase the number of pores visualized. The level of porosity detected visually using μCT was higher than any of the HR-pQCT images.

Regressions between HR-pQCT and μCT values for trabecular parameters are shown in Table II. For Tb.BMD and BV/TV, all HR-pQCT voxel sizes were strongly predictive of the μCT value (Tb.BMD: $r^2 = 0.84$–0.85; $p < 0.001$, BV/TV: $r^2 = 0.96$–0.99; $p < 0.001$). HR-pQCT measurement of Tb.N

was strongly predictive at 82 μm ($r^2 = 0.88$; $p < 0.001$) and at 41 μm using both indirect ($r^2 = 0.93$; $p < 0.001$) and direct ($r^2 = 0.94$; $p < 0.001$) analysis methods, while 123 μm data were less predictive ($r^2 = 0.77$; $p < 0.001$). A similar pattern of agreement is seen in Tb.Sp, with strong agreement at 82 μm ($r^2 = 0.91$; $p < 0.001$) and at 41 μm (direct: $r^2 = 0.95$; $p < 0.001$, indirect; $r^2 = 0.94$; $p < 0.001$) and weaker correlations at 123 μm ($r^2 = 0.78$; $p < 0.001$). For Tb.Th, indirect measures at all three voxel sizes showed weak agreement to μCT values. Direct analysis at 41 μm, however, was significantly predictive ($r^2 = 0.82$; $p < 0.001$).

Results from the RMANOVA and regressions showed trabecular analysis of HR-pQCT images at 41 μm to be most similar to μCT (Table III). No significant differences from the gold standard μCT values were found for Tb.N measured at 41 μm by direct or indirect analysis. At 82 and 123 μm, Tb.N was overestimated, with a higher degree of error at larger Tb.N values (Fig. 4). All other trabecular parameters measured at any HR-pQCT voxel size were significantly different from μCT ($p < 0.05$). Tb.BMD tended to be underestimated at all voxel sizes and displayed strong proportional error, resulting in stronger underestimation at lower mean values. BV/TV and Tb.Th showed a strong disparity between the two analysis techniques; both measures were underestimated at all voxel sizes using the standard clinical (indirect) analysis but overestimated by the direct analysis at 41 μm. For BV/TV, the direct 41 μm data showed increasing overestimation with higher values, while the indirect analyses did not display proportional error. In contrast, for Tb.Th, indirect analysis on all voxel sizes displayed proportional error while direct 41 μm data did not. For both parameters, the direct analysis at 41 μm minimized RMSCV (BV/TV = 0.02; Tb.Th = 0.02). Tb.Sp tended to be underestimated at all voxel sizes, with the values generated from the direct analysis at 41 μm closest to μCT (RMSCV = 0.05).

Correlations for the extended cortical parameters (Table IV), like those for the trabecular parameters, were strongest at 41 μm. Furthermore, RMSE for all parameters was smallest using the data at 41 μm. All voxel sizes showed similar correlations with μCT data for measures of Ct.Th ($r^2 = 0.89$–0.94; $p < 0.001$). Measures of Ct.BMD showed weak but significant agreement with respect to μCT across all voxel sizes ($r^2 = 0.41$–0.59; $p < 0.05$). For Ct.TMD, only the 41 μm data showed significant agreement to μCT ($r^2 = 0.29$; $p < 0.05$).

TABLE III. Mean and standard deviation values for trabecular parameters measured using HRpQCT and μCT.

Voxel size (μm)	Tb.BMD (mg HA/cm³)	BV/TV (%)	Tb.N (1/mm)	Tb.Sp (mm)	Tb.Th (mm)
18 (μCT)	185 ± 35	0.182 ± 0.043	1.25 ± 0.19	0.75 ± 0.15	0.17 ± 0.01
41—direct	170 ± 51[a]	0.212 ± 0.057[b]	1.26 ± 0.19	0.72 ± 0.15[a]	0.21 ± 0.01[b]
41—indirect	160 ± 52[b]	0.134 ± 0.043[b]	1.27 ± 0.21	0.71 ± 0.17[b]	0.10 ± 0.02[b]
82	158 ± 54[b]	0.132 ± 0.045[b]	1.48 ± 0.29[c]	0.62 ± 0.16[c]	0.09 ± 0.02[c]
123	152 ± 57[b]	0.127 ± 0.048[b]	1.50 ± 0.35[c]	0.62 ± 0.18[c]	0.08 ± 0.01[c]

Note: Statistical significance measured using RMANOVA. Significance indicates difference to μCT.
[a] = $p < 0.05$.
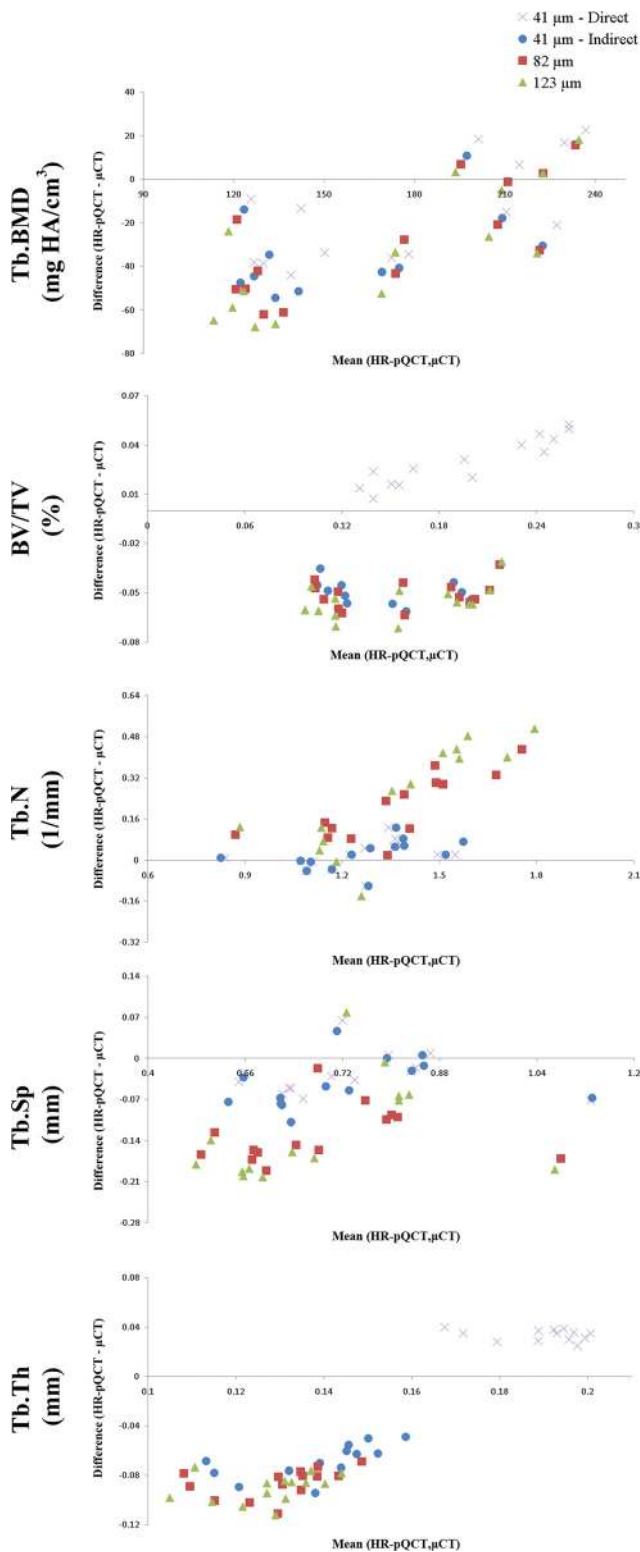[b] = $p < 0.01$.
[c] = $p < 0.001$.

FIG. 4. Bland–Altman plots for trabecular parameters.

Cortical porosity measures had a high degree of resolution dependence. The correlation for Ct.Po at 41 μm was stronger than that of the 82 μm data (41: $r^2 = 0.84$, $p < 0.001$; 82: $r^2 = 0.61$, $p < 0.03$). There was one highly porous specimen that may have influenced the Ct.Po regression at 41 μm; excluding that specimen results in an r^2 of 0.67, $p < 0.001$. For Ct.Po.Dm, only the 41 μm data were signifi-

cantly predictive of μCT values ($r^2 = 0.36$; $p < 0.05$); similarly, Ct.Po.Dm.SD values were correlated most strongly at 41 μm ($r^2 = 0.59$; $p < 0.01$).

All HR-pQCT values for the extended cortical parameters were significantly different than those generated from μCT (Table V). Measures of Ct.BMD, Ct.TMD, and Ct.Th were overestimated by all voxel sizes as shown in the corresponding Bland–Altman plots (Fig. 5). For Ct.Th, the 41 μm data had the smallest error (RMSCV = 0.08). Ct.Po was underestimated at all voxel sizes, with the 41 μm data providing the greatest accuracy (RMSCV = 0.30); all voxel sizes show a pattern of increasing underestimation with higher porosity values.

IV. DISCUSSION

This study provides further evidence of the effects of image voxel size on parameters of bone density and structure. Resolution dependence is seen in the results from both the standard trabecular analysis and the extended cortical analysis, with microstructural parameters and specifically cortical porosity measures displaying the most variation between voxel sizes. Correlations between HR-pQCT and μCT are also influenced by analysis technique, as evidenced by the results of image analysis using both direct and indirect approaches. Generally, the HR-pQCT images with the smallest voxel size (41 μm) and the direct voxel-based analysis provided the most accurate quantification of structural measures *in vitro*.

It must be noted that voxel size is not equivalent to true spatial resolution of the HR-pQCT imaging system. Therefore, though the nominal resolution is increased by a factor of two from HR-pQCT images at 82 μm to those at 41 μm, the actual increase in true spatial resolution differs, as noted in Sec. III. In addition to varying spatial resolution, the images at each voxel size also have different signal-to-noise ratios (μCT: 32.9, 41 μm: 52.4, 82 μm: 61.8, 123 μm: 83.6). It is reasonable to expect that the regression values presented here would differ if the SNR was adjusted at different voxel sizes, though it should be noted that increasing the SNR would necessitate an increase in radiation dose.

Accuracy of HR-pQCT trabecular microstructure measures is influenced by voxel size. At 123 μm, voxel dimensions approximate the thickness of individual trabecula and, as evidenced by the weaker correlations, partial volume effects become more significant. Correlations are strengthened as voxel size decreases, with the 41 μm data showing the strongest correlations, though correlations remain weak for Tb.Th ($r^2 = 0.48$). For the indirect analysis, RMSE is minimized for all trabecular structure parameters at 41 μm; smaller errors and stronger correlations for the 41 μm data demonstrate an improved degree of accuracy compared to analysis at the standard clinical voxel size of 82 μm.

The direct analysis applied to the 41 μm data yields an additional improvement in accuracy for trabecular microstructure parameters. The increase in correlation and decrease in RMSE is most evident for Tb.Th and BV/TV.

TABLE IV. Regression data for extended cortical parameters.

Voxel size(μm)	Slope	Intercept	r^2	RMSE
Ct.Th				
41	0.96	−0.04	0.94	0.051
82	1.01	−0.09	0.93	0.053
123	1.09	−0.23	0.89	0.066
Ct.BMD				
41	0.56	233	0.59	34.8
82	0.39	384	0.44	40.9
123	0.28	494	0.41	41.9
Ct.TMD				
41	0.34	474	0.29	33.0
82	0.3	509	NS	34.1
123	0.31	498	NS	33.4
Ct.Po				
41	1.15	0.03	0.84	0.018
82	1.61	0.04	0.61	0.029
123	0.83	0.06	NS	0.040
Ct.Po.Dm				
41	0.73	0	0.36	0.028
82	1.08	−0.06	NS	0.030
123	0.85	−0.04	NS	0.032
Ct.Po.Dm SD				
41	0.74	0.04	0.59	0.015
82	0.89	0.04	0.44	0.017
123	0.26	0.09	NS	0.023

The results for the 41 μm direct analysis presented here have stronger correlations to the reference values than data in the literature examining direct analysis of radius trabecular microstructure at 82 μm.[13] Specifically, the correlations for Tb.Th ($r^2 = 0.82$) and BV/TV ($r^2 = 0.99$) at 41 μm are higher than those reported by Macneil and Boyd (Tb.Th: $r^2 = 0.10$, BV/TV: $r^2 = 0.70$). This suggests that the smaller voxel size may allow for a more accurate segmentation of trabecular structure, which, in turn, results in more accurate quantification of trabecular microstructure parameters.

The conclusions drawn in this study do not necessarily instruct us as to the resolution dependence of alternate trabecular microstructure analysis techniques. Previous works in the literature, such as the volumetric topological analysis presented by Saha *et al.*[19] and the individual trabecular segmentation method presented by Liu *et al.*,[20] analyze the trabecular network in a localized, individual manner and have both reported strong correlations to μCT. The applic-

ability of these analyses to the HR-pQCT data at 123 μm warrants further study to determine the resolution dependence of these novel analyses.

Results from the extended cortical analysis for density and thickness measures show similar levels of correlation across all HR-pQCT voxel sizes. Ct.Th is overestimated at all HR-pQCT voxel sizes, most likely as a result of partial volume effects along the perimeters of the bone. The correlation of HR-pQCT Ct.Th to the reference value is weakest for the 123 μm data, presumably due to the inability to resolve thinner structures as a result of larger voxel sizes. The loss of these thinner structures results in a shift in the thickness distribution towards higher values, thus decreasing correlation to μCT. This effect is confirmed by the Bland–Altman plot, in which the 123 μm data display a bias toward higher error at lower Ct.Th values.

The results for measures of cortical porosity show a strong degree of resolution dependence. This is to be expected considering the spatial resolution necessary to distinguish individual cortical pores. Previous histological studies have reported mean Haversian pore diameters in the range of 40–600 μm from samples taken from the femur, with pores as small as 14 μm and as large as 1 mm present.[21–23] A synchrotron radiation μCT study of radius samples found median pore diameters in the range of 36 to 74 μm.[24] While the correlation for Ct.Po is improved by decreasing the voxel size ($r^2 = 0.61$ at 82 μm; $r^2 = 0.84$ at 41 μm), Ct.Po.Dm remained weakly correlated ($r^2 = 0.36$). This confirms that HR-pQCT resolutions are unable to resolve pore structure completely, further evidenced by the underestimation of Ct.Po and the overestimation of Ct.Po.Dm at all voxel sizes. Pores identified in μCT may correspond to smaller structures such as lacunae and Volksmann's canals in addition to smaller Haversian canals. HR-pQCT images, on the other hand, may be identifying larger Haversian canals as well as pathological structures consisting of merged pores. Given that different levels of pore structure are being imaged using μCT and HR-pQCT, it is likely that the correlation between these two imaging systems for measures of porosity is dependent on the distribution of pore sizes being compared. Characterization of the scale-dependency of pore structures detected using these two imaging systems deserves further investigation. Similar to the topological analysis methods developed for the trabecular network, analysis of cortical pore space on a topological

TABLE V. Mean and standard deviation values for extended cortical parameters measured using HR-pQCT and μCT.

Voxel size (μm)	Ct.Th (mm)	Ct.BMD (mg HA/cm^3)	Ct.TMD (mg HA/cm^3)	Ct.Po (-)	Ct.Po.DM (mm)	Ct.Po.DM.SD (mm)
18(μCT)	0.59 ± 0.19	735 ± 52	799 ± 38	0.10 ± 0.04	0.15 ± 0.03	0.11 ± 0.02
41	0.65 ± 0.19[c]	900 ± 73[c]	954 ± 59[c]	0.06 ± 0.03[c]	0.20 ± 0.03[c]	0.09 ± 0.02[b]
82	0.68 ± 0.18[c]	910 ± 90[c]	973 ± 61[c]	0.04 ± 0.02[c]	0.19 ± 0.02[c]	0.08 ± 0.02[c]
123	0.76 ± 0.17[c]	870 ± 122[c]	963 ± 62[c]	0.04 ± 0.03[c]	0.23 ± 0.02[c]	0.08 ± 0.02[b]

Note: Statistical significance measured using RMANOVA. Significance indicates difference to μCT.
[a] = $p < 0.05$.
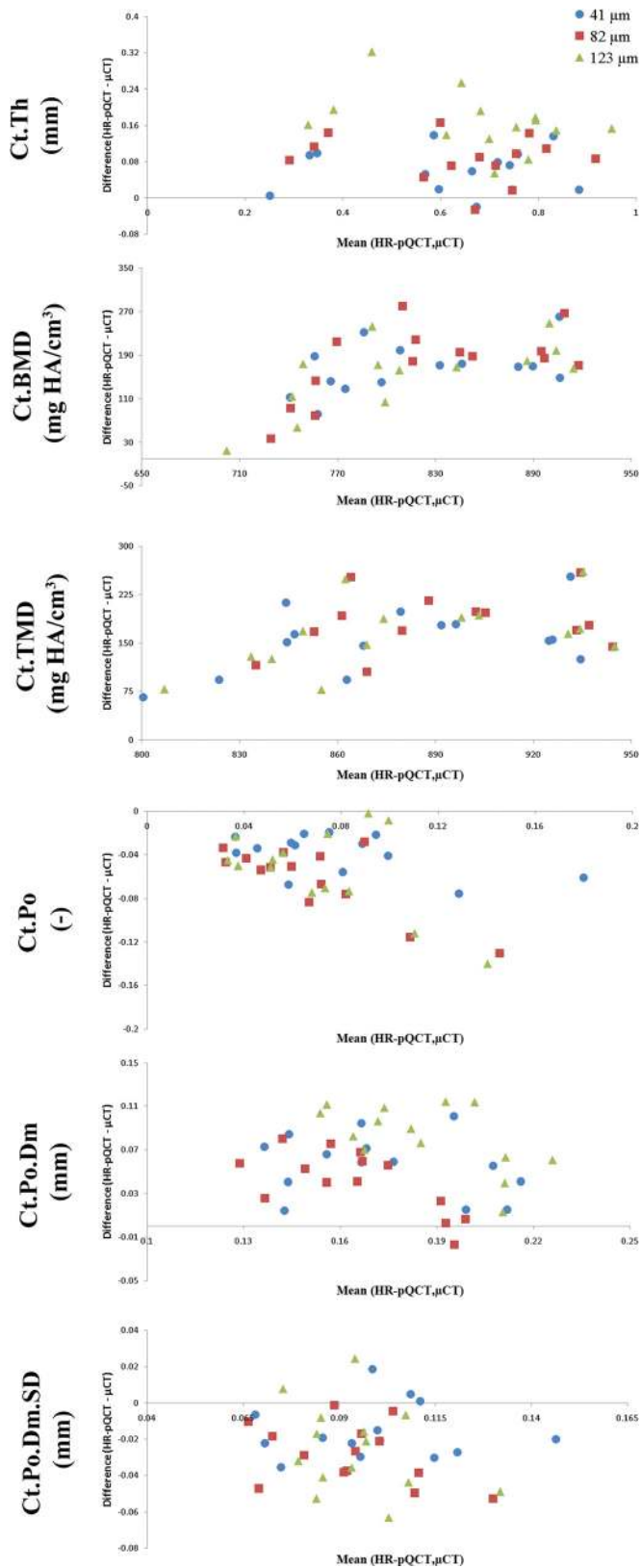[b] = $p < 0.01$.
[c] = $p < 0.001$.

FIG. 5. Bland–Altman plots for extended cortical parameters.

basis may yield further information on the microstructure of the cortical region.

In a previous study that examined radii using HR-pQCT at 82 μm,[11] correlations for Ct.Po ($r^2 = 0.80$) are stronger

than the r^2 values reported here ($r^2 = 0.61$). Discrepancies between the correlation values for the porosity measures generated in this study and those in Nishiyama *et al.*[11] are likely driven by differences in the porosity segmentation technique. In Nishiyama *et al.*,[11] cortical pores are defined as all void voxels within the cortical region produced by an automatic segmentation technique.[9] In this study, the segmented image of the cortical region is subject to further image processing operations to refine the porosity estimate, thus distinguishing intracortical pores from periosteal and endosteal void as well as transcortical foramen or erosions.[8] Considering the range of Ct.Po values reported in Nishiyama *et al.*[11] (0.08–0.25 for 82 μm HR-pQCT) are higher than those reported here, it is likely that the strength of their correlation is driven by void voxels that are not exclusively intracortical.

While every effort was made to minimize sources of error, this study is subject to several limitations. On average, the analyzed region for all samples consisted of 78% of the entire HR-pQCT data set. It is reasonable to assume that correlations for all bone parameters would be more robust if the full data set were analyzed. The strength of the correlations may also have been affected by the advanced donor age and relatively deteriorated bone quality. The results presented here, however, are applicable to a number of patient populations such as postmenopausal women and osteoporotic subjects in whom bone quality is relatively poor. Therefore, though correlations may be different for a healthy subject population, they reflect the variance in bone quality found in various sample populations studied using HR-pQCT.

Disparities between HR-pQCT and μCT densitometric measurements most likely result from differences in specimen preparation and scanner setup in addition to resolution. Specimens were scanned with marrow and minimal soft tissue intact using HR-pQCT but were cleaned of marrow and soft tissue (with the marrow space being filled with saline) prior to μCT scanning. The resulting differences in background attenuation between the HR-pQCT and μCT images partly explain the lower values of Tb.BMD measured using HR-pQCT. Additionally, substantial differences exist in the scanning environments of both imaging systems. Beam hardening correction methods differ between the two imaging systems, and phantoms used to determine the software correction factors are also different. Further, the energy spectrum is not identical for both scanners, and the HR-pQCT system utilizes a more effective low energy x-ray filter. Another significant factor to consider is variability in beam scattering, as the geometry of the x-ray source, object, and detector is substantially different between the two imaging systems.[25,26] As a result of these differences, establishing μCT as the gold standard for densitometric measurements may not be appropriate. The densitometric data presented here for the HR-pQCT and μCT imaging systems should be interpreted as a comparison of magnitudes rather than a measure of accuracy.

Results generated from the cortical analysis may also be influenced by variance in contouring. Though an automatic

technique was used to create the endosteal contours for HR-pQCT images, a subset of data sets required manual corrections if the contour failed to properly identify the entire endocortical boundary. Such manual edits may create differences between contours for the same bone at different voxel sizes, and though contouring was done by a single operator to reduce these errors, it is reasonable to expect that the contours across voxel sizes were not entirely uniform. In addition, the registration procedure may have introduced interpolation artifacts, which again contributed to slight differences in the VOI being analyzed for each sample.

Though the results for both cortical and trabecular analyses are improved with decreasing voxel size in this *in vitro* study, other considerations must be taken into account when considering HR-pQCT image acquisition at 41 μm for *in vivo* studies. HR-pQCT imaging at 41 μm requires a longer scan time (5.6 min in comparison with 2.8 min for 82 μm scans), and in terms of applicability to clinical *in vivo* studies, a longer scan increases the probability of patient motion. Motion artifacts can lead to significant error in measures of trabecular microstructure at 82 μm;[27] this problem would likely be exacerbated for scans at 41 μm. As noted earlier, 41 μm images also have a lower signal to noise ratio. The radiation dose for a 41 μm scan, however, remains low. Previous studies have reported a radiation dose of approximately 3 μSv for *in vivo* 82 μm scans with the same imaging parameters as those used in this study.[28] Considering that the 41 μm scanning profile used to image these specimens results in a milliamperes value 2.5 times higher than the milliamperes value at 82 μm, the radiation dose for 41 μm scans can be approximated to be 7.5 μSv, making it suitable for use in patient studies. The data presented here strongly motivate further investigation of *in vivo* HR-pQCT image acquisition at smaller voxel sizes than currently used.

In summary, this study provides an overview of the capability of HR-pQCT analysis to accurately measure trabecular and cortical bone parameters. Adjusted analysis parameters have been presented for segmentation and structure extraction at each voxel size. Direct analysis applied to the 41 μm data generates the highest accuracy for both trabecular and cortical parameters. Cortical porosity parameters are strongly resolution dependent, and at the standard clinical voxel size of 82 μm, measures of porosity are only moderately correlated to the gold standard μCT data. These results suggest that caution is warranted when interpreting HR-pQCT measures of cortical microstructure. Further study into the scale-dependence of cortical structure analysis is required. Considering the significant role that cortical bone plays in load-bearing, improved accuracy of cortical pore microstructure depiction will be crucial in the evaluation of bone response to disease or directed treatment.

Acknowledgments

[a)]Electronic mail: willy.tjong@ucsf.edu

[b)]Author to whom correspondence should be addressed. Telephone: +1 (415) 353-4534; Fax: +1 (415) 353-9423. Electronic mail: galateia.kazakia@ucsf.edu

[c)]Electronic mail: andrew.burghardt@ucsf.edu

[d)]Electronic mail: sharmila.majumdar@radiology.ucsf.edu

[1]NIH Consensus Development Panel on Osteoporosis Prevention, Diagnosis, and Therapy, "Osteoporosis prevention, diagnosis, and therapy," J. Am.MA **285**, 785–795 (2001).

[2]Y. Jiang, J. Zhao, E. Y. Liao, R. C. Dai, X. P. Wu, and H. K. Genant, "Application of micro-CT assessment of 3-D bone microstructure in preclinical and clinical studies," J. Bone Miner. Metab. **23 Suppl**, 122–131 (2005).

[3]A. Laib, T. Hildebrand, H. J. Häuselmann, and P. Rüegsegger, "Ridge number density: A new parameter for in vivo bone structure analysis," Bone **21**, 541–546 (1997).

[4]A. Laib, H. J. Hauselmann, and P. Ruegsegger, "In vivo high resolution 3D-QCT of the human forearm," Technol. Health Care **6**, 329–337 (1998).

[5]A. Laib and P. Ruegsegger, "Calibration of trabecular bone structure measurements of in vivo three-dimensional peripheral quantitative computed tomography with 28-microm-resolution microcomputed tomography," Bone **24**, 35–39 (1999).

[6]A. J. Burghardt, G. J. Kazakia, and S. Majumdar, "A local adaptive threshold strategy for high resolution peripheral quantitative computed tomography of trabecular bone," Ann. Biomed. Eng. **35**, 1678–1686 (2007).

[7]A. J. Burghardt, G. J. Kazakia, S. Ramachandran, T. M. Link, and S. Majumdar, "Age- and gender-related differences in the geometric properties and biomechanical significance of intracortical porosity in the distal radius and tibia," J. Bone Miner. Res. **25**, 983–993 (2010).

[8]A. J. Burghardt, H. R. Buie, A. Laib, S. Majumdar, and S. K. Boyd, "Reproducibility of direct quantitative measures of cortical bone microarchitecture of the distal radius and tibia by HR-pQCT," Bone **47**, 519–528 (2010).

[9]H. R. Buie, G. M. Campbell, R. J. Klinck, J. A. MacNeil, and S. K. Boyd, "Automatic segmentation of cortical and trabecular compartments based on a dual threshold technique for in vivo micro-CT bone analysis," Bone **41**, 505–515 (2007).

[10]T. Hildebrand, A. Laib, R. Muller, J. Dequeker, and P. Ruegsegger, "Direct three-dimensional morphometric analysis of human cancellous bone: microstructural data from spine, femur, iliac crest, and calcaneus," J. Bone Miner. Res. **14**, 1167–1174 (1999).

[11]K. K. Nishiyama, H. M. Macdonald, H. R. Buie, D. A. Hanley, and S. K. Boyd, "Postmenopausal women with osteopenia have higher cortical porosity and thinner cortices at the distal radius and tibia than women with normal aBMD: An in vivo HR-pQCT study," J. Bone Miner. Res. **25**, 882–890 (2010).

[12]X. S. Liu, X. H. Zhang, K. K. Sekhon, M. F. Adams, D. J. McMahon, J. P. Bilezikian, E. Shane, and X. E. Guo, "High-resolution peripheral quantitative computed tomography can assess microstructural and mechanical properties of human distal tibial bone," J. Bone Miner. Res. **25**, 746–756 (2010).

[13]J. A. MacNeil and S. K. Boyd, "Accuracy of high-resolution peripheral quantitative computed tomography for measurement of bone quality," Med. Eng. Phys. **29**, 1096–1105 (2007).

[14]G. J. Kazakia, B. Hyun, A. J. Burghardt, R. Krug, D. C. Newitt, A. E. de Papp, T. M. Link, and S. Majumdar, "In vivo determination of bone structure in postmenopausal women: A comparison of HR-pQCT and high-field MR imaging," J. Bone Miner. Res. **23**, 463–474 (2008).

[15]A. L. Kwan, J. M. Boone, K. Yang, and S. Y. Huang, "Evaluation of the spatial resolution characteristics of a cone-beam breast CT scanner," Med. Phys. **34**, 275–281 (2007).

[16]C. Studholme, D. L. G. Hill, and D. J. Hawkes, "An overlap invariant entropy measure of 3D medical image alignment," Pattern Recogn. **32**, 71–86 (1999).

[17]A. M. Parfitt, C. H. E. Mathews, A. R. Villanueva, M. Kleerekoper, B. Frame, and D. S. Rao, "Relationships between surface, volume, and thickness of iliac trabecular bone in aging and in osteoporosis—Implications for the microanatomic and cellular mechanisms of bone loss," J. Clin. Invest. **72**, 1396–1409 (1983).

[18]T. Hildebrand and P. Rüegsegger, "A new method for the model-independent assessment of thickness in three-dimensional images," J. Microsc. **185**, 67–75 (1997).

[19]P. K. Saha, Y. Xu, H. Duan, A. Heiner, and G. Y. Liang, "Volumetric topological analysis: A novel approach for trabecular bone classification on the continuum between plates and rods," IEEE Trans. Med. Imaging **29**, 1821–1838 (2010).

[20]X. S. Liu, P. Sajda, P. K. Saha, F. W. Wehrli, G. Bevill, T. M. Keaveny, and X. E. Guo, "Complete volumetric decomposition of individual trabecular plates and rods and its morphological correlations with anisotropic elastic moduli in human trabecular bone," J. Bone Miner. Res. **23**, 223–235 (2008).

[21]K. L. Bell, N. Loveridge, J. Power, N. Garrahan, B. F. Meggitt, and J. Reeve, "Regional differences in cortical porosity in the fractured femoral neck," Bone **24**, 57–64 (1999).

[22]D. Cooper, A. Turinsky, C. Sensen, and B. Hallgrimsson, "Effect of voxel size on 3D micro-CT analysis of cortical bone porosity," Calcif. Tissue Int. **80**, 211–219 (2007).

[23]N. J. Wachter, P. Augat, G. D. Krischak, M. Mentzel, L. Kinzl, and L. Claes, "Prediction of cortical bone porosity in vitro by microcomputed tomography," Calcif. Tissue Int. **68**, 38–42 (2001).

[24]K. Raum, I. Leguerney, F. Chandelier, M. Talmant, A. Saied, F. Peyrin, and P. Laugier, "Site-matched assessment of structural and tissue properties of cortical bone using scanning acoustic microscopy and synchrotron radiation mu CT," Phys. Med. Biol. **51**, 733–746 (2006).

[25]R. J. Fajardo, E. Cory, N. D. Patel, A. Nazarian, A. Laib, R. K. Manoharan, J. E. Schmitz, J. M. Desilva, L. M. Maclatchy, B. D. Snyder, and M. L. Bouxsein, "Specimen size and porosity can introduce error into muCT-based tissue mineral density measurements," Bone **44**, 176–184 (2009).

[26]K. Sekhon, G. J. Kazakia, A. J. Burghardt, B. Hermannsson, and S. Majumdar, "Accuracy of volumetric bone mineral density measurement in high-resolution peripheral quantitative computed tomography," Bone **45**, 473–479 (2009).

[27]J. B. Pialat, A. J. Burghardt, M. Sode, T. M. Link, and S. Majumdar, "Visual grading of motion induced image degradation in high resolution peripheral computed tomography: Impact of image quality on measures of bone density and micro-architecture," Bone **50**, 111–118 (2011).

[28]S. Boutroy, M. L. Bouxsein, F. Munoz, and P. D. Delmas, "In vivo assessment of trabecular bone microarchitecture by high-resolution peripheral quantitative computed tomography," J. Clin. Endocrinol. Metab. **90**, 6508–6515 (2005).